Kinesin-5, a mitotic microtubule-associated motor protein, modulates neuronal migration

Aditi Falnikar[a], Shubha Tole[b], and Peter W. Baas[a]
[a]Department of Neurobiology and Anatomy, Drexel University College of Medicine, Philadelphia, PA 19129;
[b]Department of Biological Sciences, Tata Institute of Fundamental Research, Mumbai 400 005, India

ABSTRACT **Kinesin-5 (also called Eg5 or kif11) is a homotetrameric motor protein that functions by modulating microtubule (MT)–MT interactions. In the case of mitosis, kinesin-5 slows the rate of separation of the half-spindles. In the case of the axon, kinesin-5 limits the frequency of transport of short MTs, and also limits the rate of axonal growth. Here we show that experimental inhibition of kinesin-5 in cultured migratory neurons results in a faster but more randomly moving neuron with a shorter leading process. As is the case with axons of stationary neurons, short MT transport frequency is notably enhanced in the leading process of the migratory neuron when kinesin-5 is inhibited. Conversely, overexpression of kinesin-5, both in culture and in developing cerebral cortex, causes migration to slow and even cease. Regions of anti-parallel MT organization behind the centrosome were shown to be especially rich in kinesin-5, implicating these regions as potential sites where kinesin-5 forces may be especially relevant. We posit that kinesin-5 acts as a "brake" on MT–MT interactions that modulates the advance of the entire MT apparatus. In so doing, kinesin-5 regulates the rate and directionality of neuronal migration and possibly the cessation of migration when the neuron reaches its destination.**

Monitoring Editor
Paul Forscher
Yale University

Received: Nov 19, 2010
Revised: Feb 14, 2011
Accepted: Mar 3, 2011

INTRODUCTION

Development of the vertebrate brain depends on the orderly migration of neurons from their sites of birth to their final destinations (Sidman and Rakic, 1973). By the time their journey is underway, migrating neurons have already ceased undergoing mitosis and have taken on a highly polarized morphology. The leading process extends in the direction of movement, after which the soma lunges forward, taking with it the nucleus. In some cases, a trailing process lags behind and is absorbed into the soma as movement ensues. The shape and polarity of the migrating neuron as well as its movement are all dependent on a functionally interconnected microtubule (MT) array that traverses the various compartments of the cell. A wealth of literature over the past several years suggests that MTs in a migratory neuron are attached at their minus ends to the centrosome, with plus ends of MTs emanating forward into the leading process and backward to engulf the nucleus (Gregory *et al.*, 1988; Schaar and McConnell, 2005). Although the specifics can vary among different types of migratory neurons (Umeshima *et al.*, 2007; Distel *et al.*, 2010), migration is generally thought to occur by a two-step process, via forces generated by cytoplasmic dynein and actomyosin (Solecki *et al.*, 2009; Martini and Valdeolmillos, 2010). First, these forces pull on the MTs in the leading process, thus yanking the centrosome forward. Then, cytoplasmic dynein moves the nucleus along the MTs engulfing it, toward the centrosome (Solecki *et al.*, 2004), while actomyosin pushes the nucleus from behind (Tanaka *et al.*, 2004; Bellion *et al.*, 2005; Schaar and McConnell, 2005; Tsai *et al.*, 2007).

The forces generated by cytoplasmic dynein can be likened to an accelerator that drives neuronal migration. Tightly controlled movements often involve a brake so that the movement can be appropriately responsive to external guidance cues and can ultimately cease. As a rule, molecular motor proteins are modulated by complementary and antagonistic relationships with other motors, as is most clearly illustrated in the mitotic spindle (Sharp *et al.*, 2000). For example, kinesin-5 (also called Eg5 or kif11) is a slow motor compared with cytoplasmic dynein, and therefore can act as a brake to modulate the separation of the half-spindles by limiting the rate at

This article was published online ahead of print in MBoC in Press (http://www.molbiolcell.org/cgi/doi/10.1091/mbc.E10-11-0905) on March 16, 2011.

Address correspondence to: Peter W. Baas (pbaas@drexelmed.edu).

Abbreviations used: CP, cortical plate; DMSO, dimethyl sulfoxide; eGFP, enhanced green fluorescent protein; IZ, intermediate zone; MT, microtubule; PBS, phosphate-buffered saline; PLL, poly-L-lysine; SVZ, subventricular zone; VZ, ventricular zone.

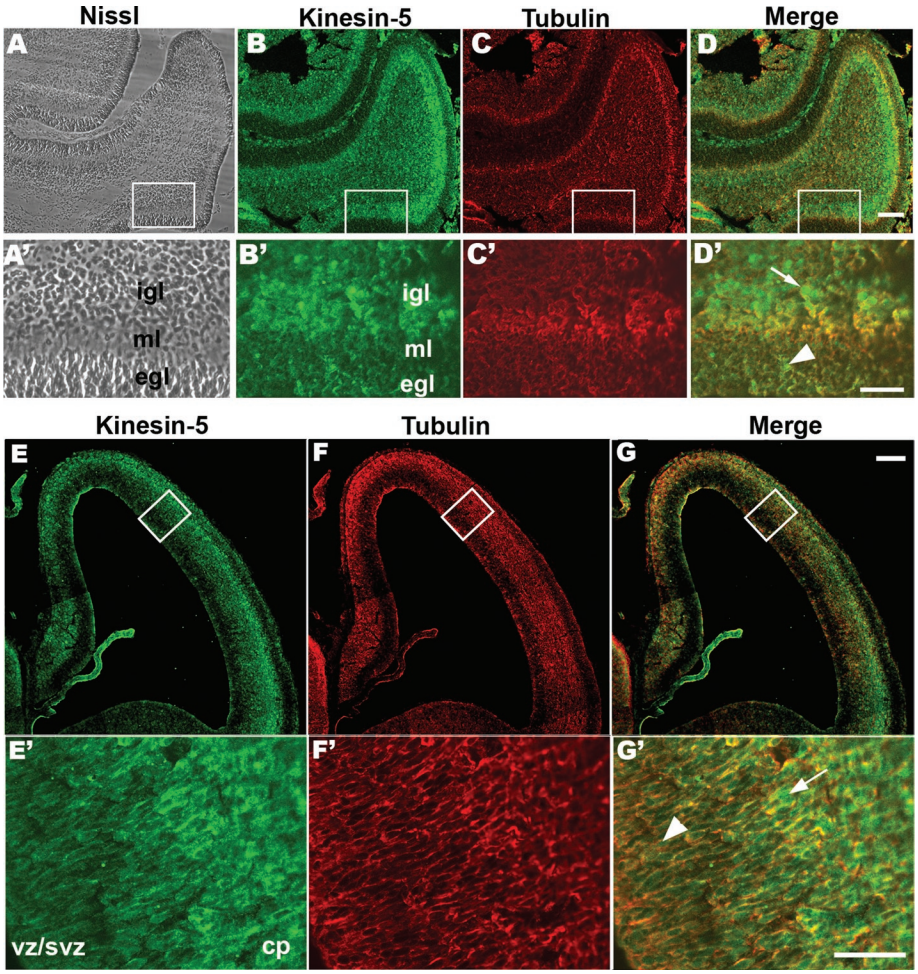

FIGURE 1: Expression of kinesin-5 protein in neonatal rat brain. (A) A sagittal section of p8 rat cerebellum stained with Nissl stain. (B) The serial section double-stained with a polyclonal total kinesin-5 antibody and (C) a monoclonal α-tubulin antibody. (D) Merge of red and green channels. Scale bar, 100 μm. Boxed areas in (A–D) are viewed at 4× the magnification in (A′–D′). Cell-dense external and internal granule layers (egl and igl, respectively) and the cell-sparse molecular layer (ml) are visible in high magnification of the Nissl-stained section (A′). Corresponding regions are indicated in the high magnification of the serial section double-stained with kinesin-5 (B′) and α-tubulin (C′) antibodies. Merge of the red and the green channel in (D′). Kinesin-5–positive cells in the egl (D′ arrowhead) and in the igl (D′ arrow). Scale bar, 50 μm. A coronal section of E16 rat cortex double-stained with the polyclonal total kinesin-5 antibody (E) and a monoclonal α-tubulin antibody (F). (G) Merge of red and green channels. Scale bar, 50 μm. Boxed areas in (E–G) are viewed at 4× the magnification in (E′–G′). The VZ/SVZ region and outer CP region (cp) are marked (E′). A kinesin-5–positive cell in the VZ/SVZ region (G′, arrowhead) and outer CP region (G′, arrow). Scale bar, 50 μm.

which cytoplasmic dynein can move the MTs apart (Saunders *et al.*, 2007).

Recent studies suggest that kinesin-5 also acts as a brake on MT–MT interactions in developing neurons. Depletion or inhibition of kinesin-5 from cultured sympathetic neurons results in an axon that grows faster (Haque *et al.*, 2004; Yoon *et al.*, 2005; Myers and Baas, 2007) but does not turn properly (Nadar *et al.*, 2008). Frequency of MT transport in the axon is enhanced when kinesin-5 is inhibited and MTs extend deeper into growth cones with a less polarized distribution. These effects are explicable, at least in part, by kinesin-5's capacity to oppose cytoplasmic dynein. In the present study, we sought to investigate whether kinesin-5 could modulate MT–MT interactions in the migratory neuron and whether such effects could influence the movement of the neuron and perhaps the cessation of movement when the neuron reaches its final destination. In addition to enhancing our understanding of the normal developmental process, these studies may also be relevant to congenital diseases that arise from flaws in neuronal migration that are often caused by mutations in genes relating to the MT cytoskeleton (Keays *et al.*, 2007; Jaglin and Chelly, 2009; Jaglin *et al.*, 2009).

RESULTS

Kinesin-5 levels are highest when migrating neurons have reached their destination

Our initial discovery of kinesin-5 in terminally postmitotic neurons consisted of in situ hybridization analyses indicating strong expression of kinesin-5 mRNA in various populations of neurons in the developing brain, including migratory neurons in the cerebral cortex and cerebellum (Ferhat *et al.*, 1998). These studies showed that the highest mRNA levels for kinesin-5 are present in migratory neurons early in their journey (Ferhat *et al.*, 1998). Protein levels do not always coincide precisely with mRNA levels, however, and it is possible that an increase in the former might lag behind an increase in the latter. For this reason, we wanted to begin our present studies on neuronal migration by conducting immunohistochemistry for kinesin-5 on developing brain. For these analyses (and also for Western blotting; see below), we used the same anti–kinesin-5 antibody that was used in our recent studies on growth cones (Nadar *et al.*, 2008). The results were confirmed with one other kinesin-5 antibody (unpublished data).

The immunohistochemistry revealed that, in the p6 rat cerebellum, the protein levels for kinesin-5 are particularly high in the outer regions of the inner granule layer (Figure 1, B and D). Higher magnification images revealed that the cells in the outer granule layer also express kinesin-5 (Figure 1D′, arrowhead), but the cells in the inner granule layers are stained more intensely (Figure 1D′, arrow). Because birth-dating studies have established that the granule neurons migrate from the outer granule layer, past the Purkinje layer, to settle into the most superficial region of the inner granule layer (Altman, 1969), we would conclude from these results that kinesin-5 is present throughout the journey but is present at particularly high levels when the journey is complete. Developing cerebral cortex exhibited a consistent expression pattern. In cortex, kinesin-5 immunostaining was most intense in outer regions of the cortical plate (Figure 1, E and G). Cells in the ventricular zone (VZ) and subventricular zone (SVZ) were weakly stained for kinesin-5 (Figure 1G′, arrowhead), whereas cells in the outer cortical plate region displayed strong staining (Figure 1G′, arrow). During corticogenesis, after proliferation at the region along the ventricles (VZ), the neurons become postmitotic and migrate out. Neurons are born in an orderly progression, with later born neurons migrating past the earlier born neurons and settling in more

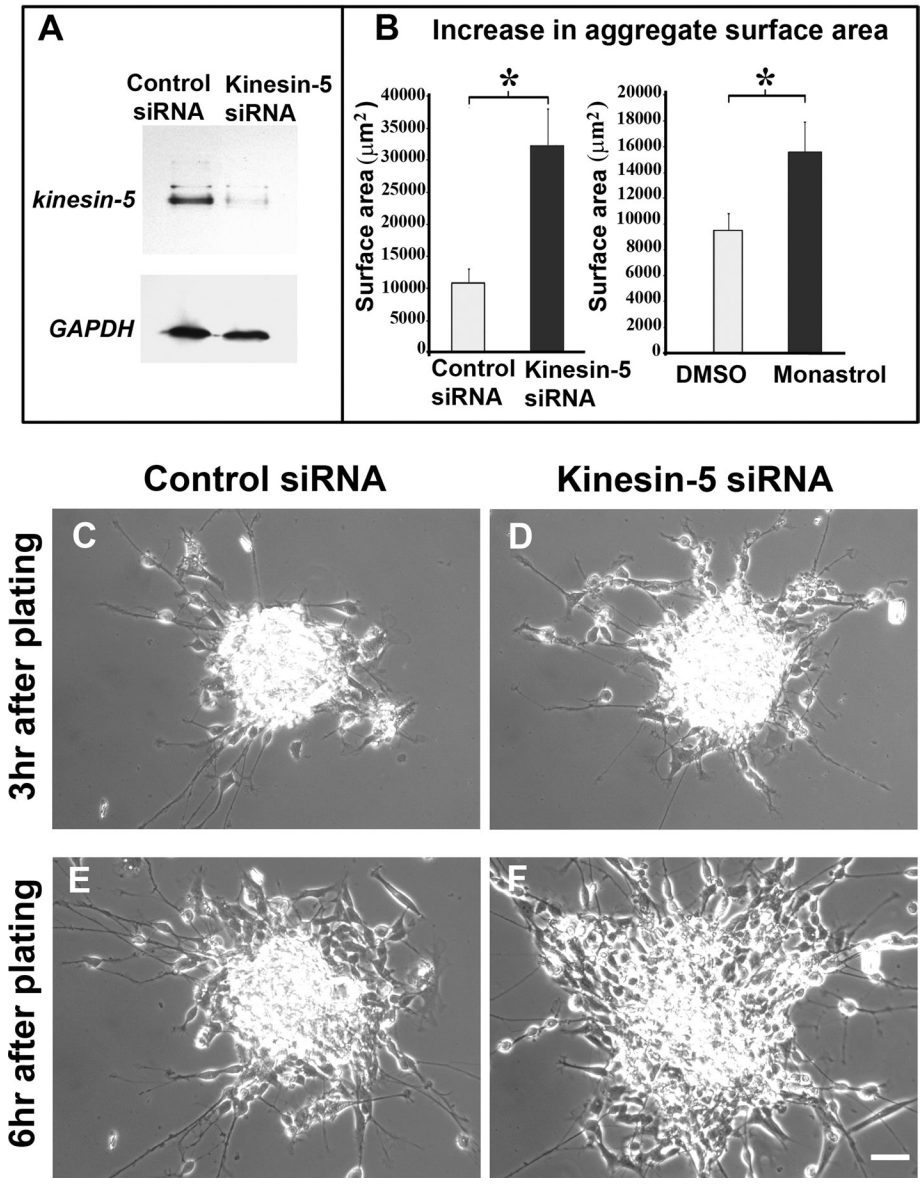

FIGURE 2: Inhibition of kinesin-5 accelerates neuronal migration. (A) Western blot in top panel showing kinesin-5 protein levels in cultured neurons treated with control siRNA and kinesin-5 siRNA, respectively. Glyceraldehyde-3-phosphate dehydrogenase (GAPDH) loading control for both protein samples is shown in the bottom panel. (B) Mean increase in the surface area of aggregates treated with control siRNA and kinesin-5 siRNA within 3 h and mean increase in the surface area of aggregates treated with 0.1% DMSO and 100 μM monastrol within 3 h. (C and E) Phase-contrast images of a cerebellar reaggregate treated with control siRNA at 3-h and 6-h points after plating, respectively. (D and F) Similar images of a reaggregate treated with kinesin-5 siRNA show notable increase in the rate of disaggregation as a result of kinesin-5 depletion. Scale bar, 25 μm.

superficial layers. In this way, cortical laminae are built by an "inside-first and outside-last" neurogenic gradient (Sheppard and Pearlman, 1997). Thus our results in two different migratory neuronal populations confirm that kinesin-5 is present in migratory neurons and that its levels are highest at the cessation of the migratory journey.

Inhibition of kinesin-5 accelerates neuronal migration

Several different in vitro culture systems have been used over the years for functional studies on neuronal migration. None ideally recapitulates the mechanisms of migration in the three-dimensional environment of the brain, with its complexity of factors and cell types that influence and direct migration. For our studies, it was necessary to use flattened cells on glass for high-resolution microscopy, and it was necessary to use a system in which numbers of cells were sufficiently high so that transfections could be performed under a number of different conditions before plating. Therefore we chose to use an in vitro culture system of rat cerebellar granule neurons that has been used in the past to study the cytoskeletal mechanisms underlying neuronal migration (Bix and Clark, 1998; Hirotsune *et al.*, 1998; He *et al.*, 2010; Peng *et al.*, 2010; Tahirovic *et al.*, 2010). In this system, cerebella are dissociated, and then the cells are allowed to form aggregates by being incubating in a polypropylene tube before plating on laminin-coated glass. Neurons then migrate out of the aggregate in a radial manner that can be quantified. This preparation is a mixed-cell one in which some nonneuronal cells are present and presumably contribute growth factors, but wherein the migratory neurons move mainly against one another as well as the substrate (see *Materials and Methods*). More than 90% of the cells in these cultures were determined to be neurons, on the basis of staining for neurofilament proteins (unpublished data). Although this system is sufficient for our purposes here, it is worth noting that it does not as faithfully reflect the conditions of migration in the brain as do certain other in vitro migration systems, such as those designed to enable cerebellar granule neurons to migrate along glial processes (Hatten and Mason, 1990).

To suppress kinesin-5 function, we used siRNA to gradually deplete the kinesin-5 protein as well as monastrol, a drug that acutely inhibits the ability of kinesin-5 to hydrolyze ATP (Cochran and Gilbert, 2005). The effects of the siRNA used for these studies were previously shown to be reversible by restoring kinesin-5 levels in other types of neurons (Myers and Baas, 2007). Seventy-two hours is sufficient time for the siRNA to deplete >85% of the kinesin-5 protein as determined by Western blotting (see Figure 2A). In our experience, transfection of siRNA with the Nucleofector device (Amaxa Biosystems, Lonza, Cologne, Germany) results in transfection of virtually all of the neurons as assessed by immunostaining (He *et al.*, 2005). (The nonneuronal cells would presumably also cease expression of kinesin-5, which might reduce their number over time as mitosis is suppressed, possibly altering the complement of growth factors in the culture. This is one reason why we also conducted studies with monastrol, which elicits its effects in a more acute manner.) As the neurons begin to migrate out of the aggregate, the tightly clumped aggregate is converted into a loose mass of cells, thus initially causing an increase in the size of the aggregate (e.g., compare Figure 2, C and E).

We chose similarly sized aggregates for comparison and monitored their surface area (in μm^2) at two time points: 3 h after plating and 6 h after plating. We calculated the difference between the surface areas at these time-points and compared the means of these differences between control siRNA and kinesin-5 siRNA groups.

Nine kinesin-5-siRNA–transfected aggregates exhibited an average 32,135.4 μm^2 increase in surface area (SEM = 5899.5), whereas 11 control siRNA-transfected aggregates exhibited only an average 10,821.3 μm^2 increase (SEM = 2138.28) within 3 h, which was statistically significant ($p = 0.0018$, Figure 2B) (see representative examples in Figure 2, C–F). Similarly, 18 dimethyl sulfoxide (DMSO)-treated aggregates were compared with 14 monastrol-treated aggregates. Whereas the monastrol-treated aggregates exhibited an average 15,594.5 μm^2 increase in surface area (SEM = 2305.26), the DMSO-treated aggregates exhibited only an average 9489.2 μm^2 increase (SEM = 1288.63). This difference was found to be statically significant ($p = 0.02$, Figure 2B).

We next used live-cell imaging to track migration of individual neurons, again using both siRNA and monastrol. Images were gathered of migrating neurons with a classic bipolar morphology at either 2- or 3-min intervals for a total of 4 h. Frames in which the given neuron was changing its direction of migration or was stalled due to obstacles (such as processes of the surrounding cells) were not considered for quantification. In our culture system, a subpopulation of neurons was always stationary, exhibiting speeds <10 μm/h. This population was also not considered for quantification. Typically, neurons depleted of kinesin-5 using siRNA or in which kinesin-5 activity was inhibited using monastrol moved faster than the control groups (see Figure 3, A and B; also see Supplemental Video 1, showing migration of these two cells, cell movement plot for these two cells in Figure 3C). Average speed was calculated by dividing the total distance traveled by a neuron by the time taken for the movement to occur. Whereas kinesin-5–depleted neurons migrated with an average speed of 66.1 μm/h (SEM = 3.24, N = 9), the control neurons migrated with an average speed of 34.3 μm/h (SEM = 1.53, N = 9, $p < 0.0001$). Whereas the average speed of the monastrol group was 60.5 μm/h (SEM = 2.62, N = 13), that of the DMSO group was 29.6 μm/h (SEM = 2.03, N = 10, $p < 0.0001$) (see Figure 3D). Thus inhibition of kinesin-5 produced an almost twofold increase in the average speed of migrating

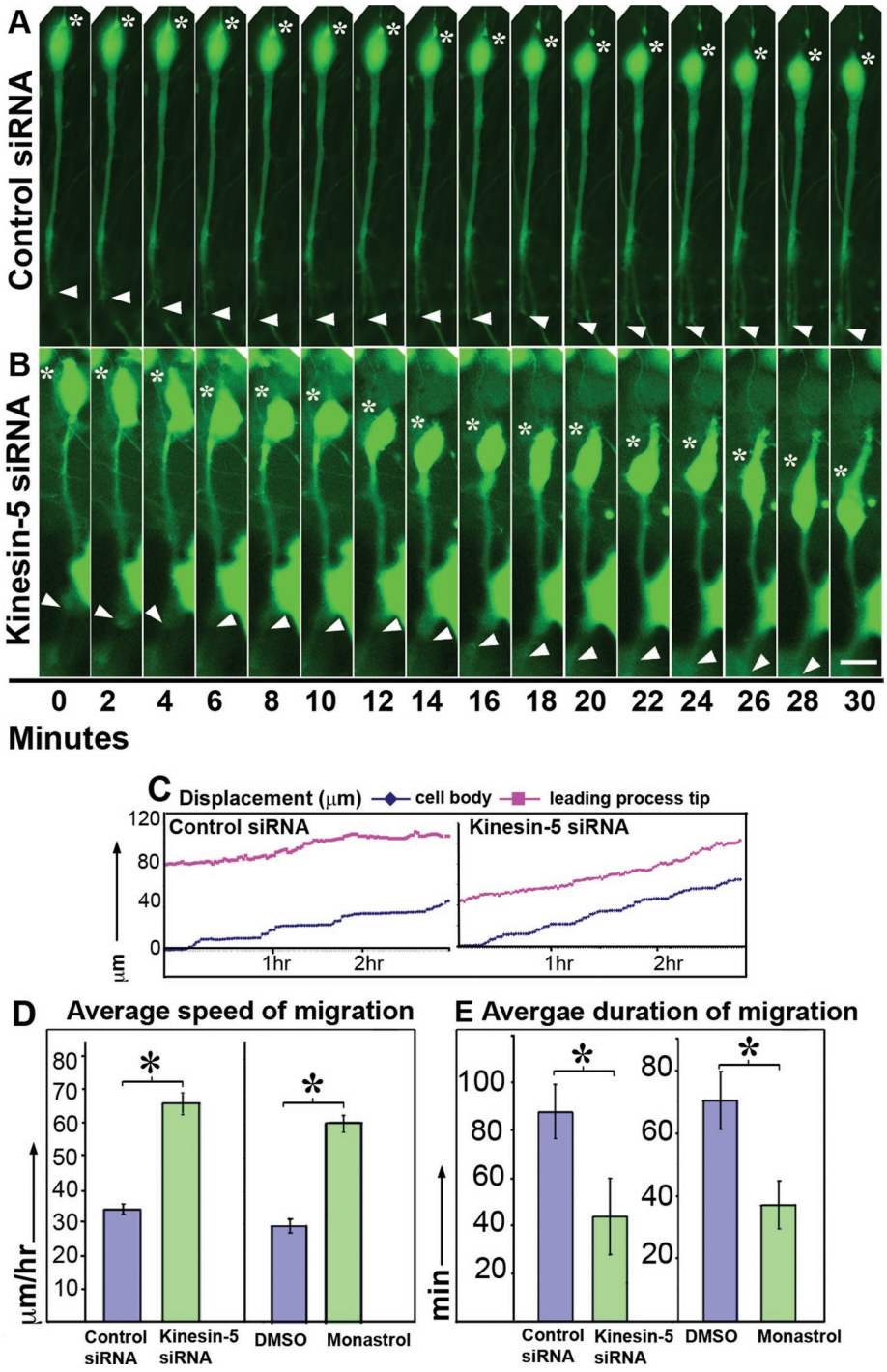

FIGURE 3: Inhibition of kinesin-5 doubles the average speed of neuronal migration and decreases the average duration of migration. (A and B) Time-lapse, phase-contrast images of migrating granule neurons transfected with control siRNA (top panel) and kinesin-5 siRNA (bottom panel). Movement of the soma and leading process tip are indicated by asterisks and arrowheads, respectively. Scale bar, 10 μm. (C) Movement plots for the soma (blue) and the leading process (magenta) of these two cells are shown. Each point represents the distance between the distal end of the soma or the tip of the leading process at a given time-point, and the position of the distal end of the soma at time-point zero. The *x*-axis represents the time elapsed since the beginning of the movie. (D) Quantification of average speed of migration for control siRNA– or kinesin-5 siRNA–transfected neurons (n = 9 in each group), and identical quantification for DMSO-treated or monastrol-treated neurons (n = 13 and 10, respectively). (E) Quantification of average duration for which neurons exhibited persistent forward movement when treated with control siRNA or kinesin-5 siRNA (n = 9 in each group), and identical quantifications for DMSO-treated or monastrol-treated neurons (n = 13 and 10, respectively).

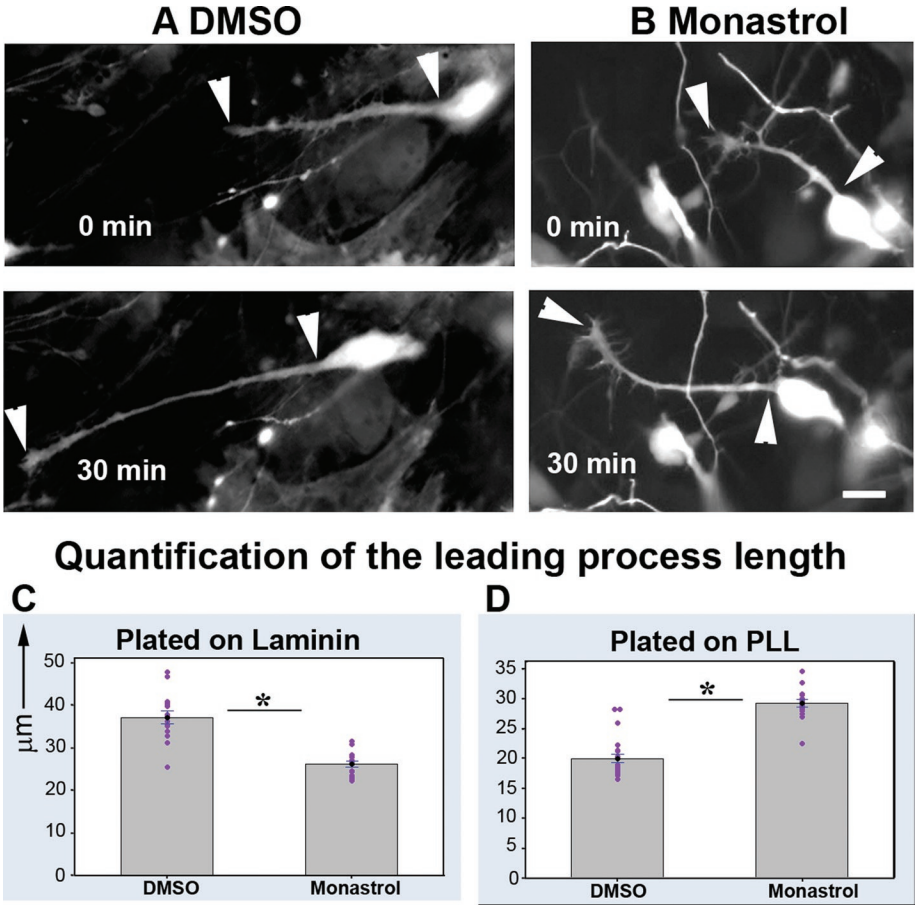

FIGURE 4: Inhibition of kinesin-5 affects the length of leading process. (A and B) Leading processes (indicated by arrowheads) of neurons treated with DMSO or monastrol, respectively. These neurons were plated on laminin, and migration was recorded for a period of 30 min. Images captured at the beginning of this period and the end of this period are shown in the top and bottom panels, respectively. Scale bar, 10 µm. (C and D) Quantification of leading process lengths, of DMSO-treated and monastrol-treated neurons, plated on laminin and PLL, respectively.

neurons. The average speed of the control siRNA-transfected or DMSO-treated neurons was similar to previous reports of migration speeds of these neurons (He *et al.*, 2010).

In our culture system, neurons undergo a phase of active forward movement followed by a relatively stationary period of little or no movement. The duration of each phase is variable with respect to individual neurons. We observed that whereas control neurons exhibited prolonged periods of active forward movement, these periods for kinesin-5–depleted neurons were shorter. Average duration of migration for control siRNA-treated neurons was 87.8 min (SEM + 11.3, N = 9), whereas that for kinesin-5 siRNA-treated neurons was 43.9 min (SEM + 15.9, N = 9, p = 0.039). Average duration of migration for DMSO-treated neurons was 70.7 min (SEM + 9.3, N = 10) whereas that for monastrol-treated neurons was 37.2 min (SEM + 7.6, N = 13, p = 0.01) (see Figure 3E).

During the course of these studies, we noticed that some of the monastrol-treated neurons started migrating in the outward direction, away from the aggregate, then paused, extended a process in the opposite direction, and then migrated back again—toward the aggregate. For example, in one instance, while five migrating neurons continuously moved away from the aggregate, three neurons started moving outward, then reversed and moved back inward (see Supplemental Video 2). We did not observe neurons reversing direction in the DMSO-treated group during the course of our recording.

Forward movement of the cell bodies of granule neurons in our culture system is sometimes known to consist of small yo-yo-type bidirectional steps (Liesi, 1992). In monastrol-treated cultures, this type of behavior of cell bodies was reduced (unpublished data).

Effects of kinesin-5 inhibition on development of the leading process

To meaningfully examine the effects of kinesin-5 on the length of the leading process (which is normally quite variable), we conducted live-cell imaging on migrating neurons for a period of at least 30 min. For a given neuron, we measured the leading process length every 5 min and averaged these values to give a single value representing the length of the leading process for that neuron. We found that the leading processes of monastrol-treated neurons exhibited an average length of 26.1 µm, whereas those of the DMSO group were 37.1 µm (n = 15 in each group, SEM = 0.73 and 1.46 respectively, $p < 0.0001$). Thus the leading processes of monastrol-treated neurons were significantly shorter than those of DMSO-treated neurons (e.g., Figure 4, A and B; quantification, Figure 4C)

This effect, to shorten the leading process, is precisely the opposite of what was observed in earlier studies on axons, which become longer when kinesin-5 wa inhibited (Haque *et al.*, 2004; Myers and Baas, 2007). We considered the possibility that the leading process may actually grow faster when kinesin-5 is inhibited, but that somal movement may also advance more quickly, thus resulting in a shorter rather than a longer leading process. To address this issue, we plated migrating neurons on a surface of poly-L-lysine (PLL) instead of laminin. To stimulate process outgrowth, laminin (2.5 µg/ml) was added *after* the neurons had adhered. Under these conditions, neurons were not able to migrate (unpublished data). We compared leading process lengths of 18 monastrol-treated neurons plated on PLL to those of 23 DMSO-treated neurons plated on the same substrate. We found that leading processes of monastrol-treated neurons were now significantly longer than those of DMSO-treated neurons. Whereas the processes from the monastrol-treated neurons displayed an average length of 28.9 µm, those from DMSO-treated neurons had an average length of 19.68 µm (SEM = 0.58 and 0.7, respectively, $p < 0.0001$; quantification, Figure 4D).

Overexpression of kinesin-5 slows neuronal migration and affects leading process development

As indicated by the immunocytochemistry of developing brain, the levels of kinesin-5 climb during the migratory journey to reach their maximum levels as the neurons reach their final destination. The depletion and inhibition studies presented thus far support a potential cause-and-effect relationship between kinesin-5 levels and the slowing/cessation of neuronal migration, but a more direct test

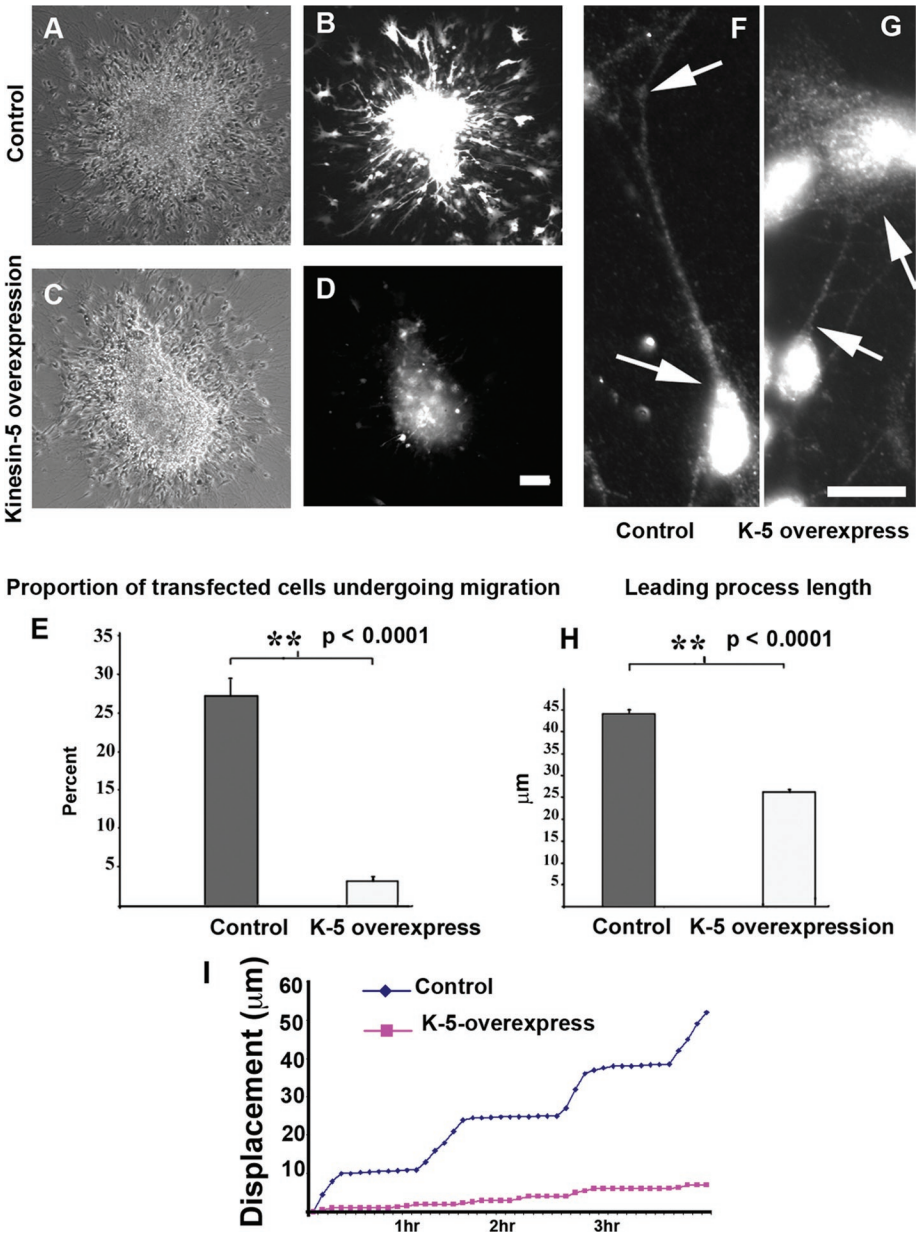

FIGURE 5: Kinesin-5 overexpression suppresses migration and alters the length of the leading process. (A and C) Phase-contrast images of eGFP and eGFP–kinesin-5–transfected aggregates, respectively. (B and D) Images of the same two aggregates through fluorescence channel showing numerous eGFP-transfected but few eGFP-kinesin-5–transfected cells migrating out of aggregate. Scale bar, 40 µm. (E) Quantification of percent transfected cells in each group. (F and G) Representative examples of leading processes of eGFP-transfected neurons (arrows, F) and eGFP–kinesin-5–transfected neurons (arrows, G), respectively. Scale bar, 5 µm. (H) Quantification of leading process length in the two groups. (I) Movement plots of live-cell imaging indicating displacement of soma of an eGFP-expressing cell (blue line) and a kinesin-5—eGFP–expressing cell (magenta line).

would be to see whether overexpressing kinesin-5 results in slowing of neuronal migration. We began these analyses in culture by using the inverse approach on the same experimental paradigm used for the depletion/inhibition studies. In this case, the cerebellar granule neurons were transfected with kinesin-5—enhanced green fluorescent protein (eGFP) or eGFP constructs, plating densely for ~24 h, and then replated on laminin to stimulate migration. Similarly sized aggregates were compared. We noticed that fluorescence intensity of kinesin-5—eGFP–transfected cells was much lower than that of eGFP-transfected cells. A mean of 27.09% of all migrating cells was transfected with eGFP (SEM = 2.4), compared with a mean of 3.09% of all migrating cells that were transfected with kinesin-5–eGFP (SEM = 0.2, $p < 0.0001$, Figure 5E). Bright-field images showed normal migration of neurons out of the aggregate, but fluorescence imaging revealed that eGFP–kinesin-5–transfected neurons were unable to leave the aggregates (Figure 5, A–D; n = 4 aggregates in each group). Live-cell imaging revealed that neurons overexpressing kinesin-5 paused throughout the course of the recording, whereas eGFP–transfected (control) neurons exhibited normal migration on laminin (n = 4 for each group, Figure 5I). Thus, whereas kinesin-5 inhibition speeds migration, its overexpression suppresses migration.

We next performed studies to assess leading process development in migrating neurons overexpressing kinesin-5 on laminin. Because kinesin-5 overexpression suppresses migration even on laminin, there was no reason to switch substrates for these studies. In 20 eGFP-transfected neurons, the average length of the leading process was 44.01 µm, and in 17 eGFP-kinesin-5–transfected neurons, it was 26.17 µm ($p < 0.0001$) (see Figure 5, F and G; quantification, Figure 5H). Thus kinesin-5 suppression produced longer leading processes, and kinesin-5 overexpression produced shorter leading processes. We should note that although the overexpressing neurons showed decreased migration and shorter leading processes, there were no signs that the overexpression produced toxic ill effects or alterations in the cells that could not be reversed with monastrol treatment. Providing additional confidence against nonspecific toxicity, dominant-negative constructs produce the opposite phenotype as the wild-type construct when expressed in neurons at equivalent levels (Myers and Baas, 2007; Nadar and Baas, unpublished data).

Overexpression of kinesin-5 slows neuronal migration in vivo

The cell culture approach was necessary for the studies presented thus far because of the high degree of resolution they afford as well as the ease of conducting drug studies, depletion studies, and overexpression studies a in parallel manner. Neuronal migration, however, is a phenomenon that is not recapitulated in all of its complexity in the culture dish, so we wished to conduct a set of studies using a widely accepted and powerful in vivo approach. For this, we used in utero electroporation to manipulate kinesin-5 expression in populations of migratory neurons. The expectation would be that neurons overexpressing kinesin-5 would migrate slower and stall along their journey. For these experiments, we expressed eGFP–kinesin-5 or eGFP as the

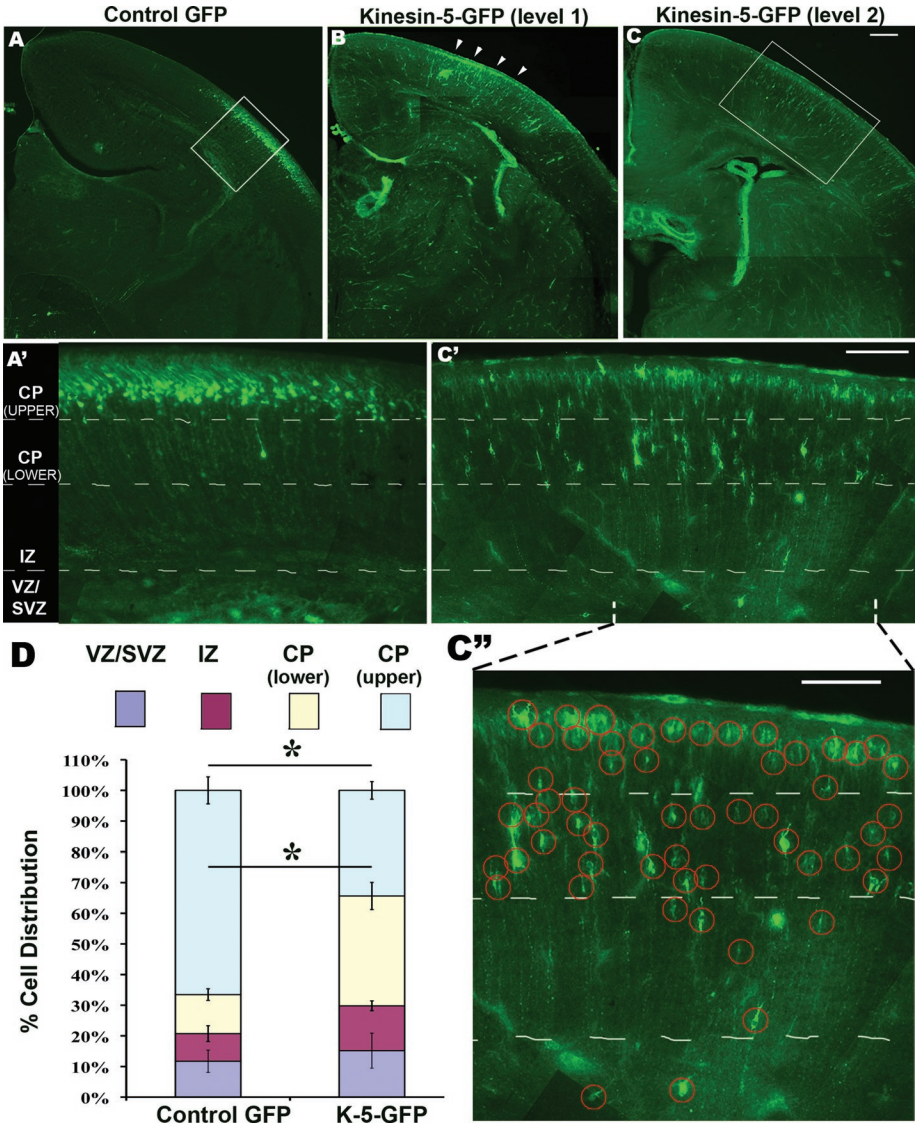

FIGURE 6: Ectopic expression of kinesin-5 affects neuronal migration in developing cerebral cortex. (A–C) Coronal sections at various levels from mouse brains electroporated with eGFP or eGFP–kinesin-5 at E14.5 and killed at P1. Electroporated region in B is indicated (arrowheads). Scale bar, 25 μm. (A′ and C′) Boxed regions in A and C viewed at higher magnification. (C″) Indicated part of C′ is enlarged, and electroporated neurons are circled. Scale bar in (C′) and (C″), 50 μm. (D) Quantification of cell distribution in the four bins. Error bars represent SEM. Note the difference in the cell distribution in the top two bins ($CP_{(upper)}$ and $CP_{(lower)}$) between the eGFP and kinesin-5–eGFP groups, *t* test p = 0.0021 and 0.0014, respectively. For the eGFP group, n = 5 brains, total 1408 cells from 10 sections were counted. For the kinesin-5–eGFP group, n = 3 brains, total 1016 cells from 18 sections were counted. The phenomenon of slowed migration was observed at all levels through the developing brain.

control in VZ neural progenitors in E14 mouse cortex. Brains were harvested at P1 by which time cells born at E14 usually reach their final positions in the superficial layers of the cortical plate. The distribution of eGFP-positive cells was quantified in coronal sections in the kinesin-5 and control groups (see Figure 6, A–C). Specifically, we counted cells in four bins—VZ/SVZ, intermediate zone (IZ), lower cortical plate (CP), and upper CP (Figure 6, A′ and C′).

The results indicate that while the majority of GFP-transfected VZ neural progenitors migrated to the outer cortical layers, kinesin-5–overexpressing progenitors were less organized, with significantly more occupying the lower CP bin, suggesting slower migration. In the control group, 66.6% of cells (SEM = 4.42) were in the upper CP, whereas in the overexpressing group 34.4% of cells (SEM = 2.89) were in this bin (p = 0.0021). In the control group, 12.7% of cells (SEM = 1.89) were in the lower CP, whereas in the overexpressing group, 35.8% of cells (SEM = 4.443) were in this bin (p = 0.0014). No significant difference was found in the counts of the other two bins in the control group (IZ: 9.02% cells, SEM = 2.57; VZ/SVZ: 11.7% cells, SEM = 3.65) and in the overexpressing group (IZ: 14.7% cells, SEM = 1.61; VZ/SVZ: 15.2% cells, SEM = 5.71) (quantification, Figure 6D). Our results with the control construct are comparable with previously reported results using this technique (Tsai *et al.*, 2005). The morphology of cells overexpressing kinesin-5 was generally similar to control cells at every stage in their journey, suggesting the perturbed migration is not caused by abnormal cellular morphology.

Kinesin-5 inhibition increases the frequency of MT transport

Mechanistic models for neuronal migration generally assume that most or all of the MTs are attached at their minus ends to the centrosome (Tsai and Gleeson, 2005). These models are based on the premise that MTs form a structural framework against which or through which cytological structures move. Little consideration has been given to the possibility that movements of MTs themselves contribute to neuronal migration, as is the case in the mitotic spindle and also the axons of postmigratory neurons. In these cases, cytoplasmic dynein not only moves cargo along MTs, it also generates forces between neighboring MTs and between MTs and the actin cytoskeleton (Hasaka *et al.*, 2004; He *et al.*, 2005). These forces rapidly transport short MTs, while also generating tensile and compressive interactions between longer MTs that can affect whether an axon grows or retracts (Myers *et al.*, 2006). Thus the impact of a molecular motor on short MT transport is a quantifiable indicator of its impact on the entire MT array. In the axon, inhibition of kinesin-5 results in a doubling of the frequency of short MT transport frequency, in both directions (Myers and Baas, 2007). This result is consistent, at least in part, with the forces of kinesin-5 opposing the forces of cytoplasmic dynein. Here, for the first time, we sought to ascertain whether the leading process of migratory neurons also contains a population of short mobile MTs, not attached to the centrosome, and, if so, whether inhibition of kinesin-5 similarly impacts the frequency of this transport.

As in our earlier studies on axons, we used the photo-bleach method for revealing MT transport (Figure 7, A–C). After bleaching a 15-μm stretch of the leading process of a neuron expressing eGFP-tubulin, we captured serial images at an interval of 2 s, for a total of 3 min. Using phase-contrast optics, we also documented

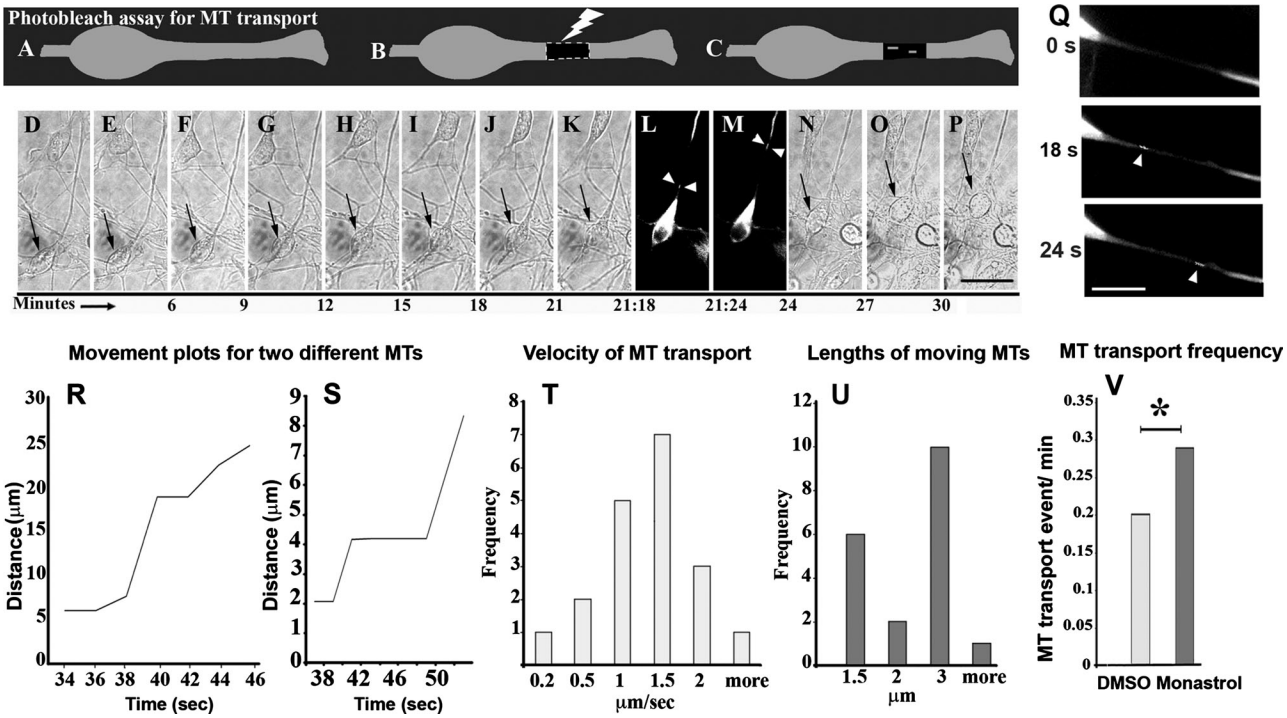

FIGURE 7: Real-time imaging reveals transport of short MTs in the leading process. In the photo-bleach assay, cultured migrating neurons expressing eGFP–tubulin (A) are exposed to a laser to create a bleached zone in the leading process (B). MTs moving from the proximal unbleached region to the distal region are visible against the dark background of the bleached zone (C). (D–K) and (N–P) Phase-contrast, time-lapse images track migration of an eGFP–tubulin–transfected neuron (black arrows) before and after photo-bleaching. (L and M) Fluorescence, time-lapse images reveal transport of short MTs (white arrowheads) through the bleached zone. Scale bar, 10 μm. (Q) Magnified images showing the bleached region at zero time-point (top panel), and a short MT moving through the photobleached zone (middle and bottom panels, arrowheads). Middle and bottom panels are magnified views of L and M, respectively. Scale bar, 10 μm. (R and S) Movement plots for two different anterogradely moving MTs are shown. Each point represents the position of the MT from the proximal end of the bleached zone, measured along the leading process. The *x*-axis represents the time elapsed since the beginning of the movie. (T) Frequency histogram of average velocities in μm/s of 19 MTs. (U) Frequency histogram of lengths of 19 MTs. (V) MT transport frequency is significantly higher in monastrol-treated neurons (13 events in 45 min) compared with DMSO-treated neurons (6 events in 30 min).

migration of the neuron before and after it was exposed to the laser. In a migrating neuron, if all the MTs are bound to the centrosome, and no free MTs exist, we would not observe movement of short MTs through the bleached zone. In contrast, if there are any short mobile MTs present, we should detect them as they transit through the bleach zone (Figure 7C).

In a neuron that was actively migrating (Figure 7, D–K and N–P, arrow), we were able to record instances of short MTs moving through the bleached zone (Figure 7, L and M, arrowheads; magnified in Q, arrowheads, middle and bottom panels, respectively). A total of 19 anterograde MT transport events were recorded during a total 102 min of image acquisition, for an average frequency of 0.190 events/min. These MTs sometimes paused and sometimes traveled at rapid speeds, with an average velocity of 1.03 μm/s (SEM, = 0.124). Individual average MT velocities are represented in Figure 5T. Lengths of moving MTs are shown in Figure 7U. Movement plots for two different MTs are shown in Figure 7, R and S.

Notably, observations of MT transport in the leading process of the migratory neurons were not entirely the same as those reported in previous studies on the axons of sympathetic and hippocampal neurons. Although the velocity of transport is essentially the same (~1 μm/s), the frequency of transport is less than one-fourth that in axon (0.752 events/min). In addition, the MT movement in the leading process is exclusively in the anterograde direction, whereas MTs move bidirectionally in axons (roughly 2/3 and 1/3 anterograde and retrograde, respectively) (Wang and Brown, 2002). This observation is particularly interesting because the leading process of cerebellar granule neurons is known to become the axon of these cells (Altman and Bayer, 1996).

We next studied the impact of kinesin-5 inhibition on MT transport in the leading process. In DMSO-treated neurons, the frequency of MT transport was the same as that in untreated cells—0.2 events/min (6 events in 30 min of image acquisition). In monastrol-treated neurons, the frequency was found to be ~1.5-fold higher—0.29 events/min (13 events in 45 min of image acquisition, $p = 0.02$) (see Figure 7V). The directionality of MT transport was unchanged, as retrograde transport of MTs was never observed in either monastrol-treated or DMSO-treated groups. Also, the average velocity of transport remained similar—1.15 μm/s and 1.03 μm/s in monastrol-treated and DMSO-treated groups, respectively (SEM = 0.44 and 0.41 in monastrol and DMSO groups, $p = 0.844$, not significant). As is the case with the axon, these results indicate that kinesin-5 restricts the number of moving MTs in the leading process, but does not impact the velocity or directionality of transport.

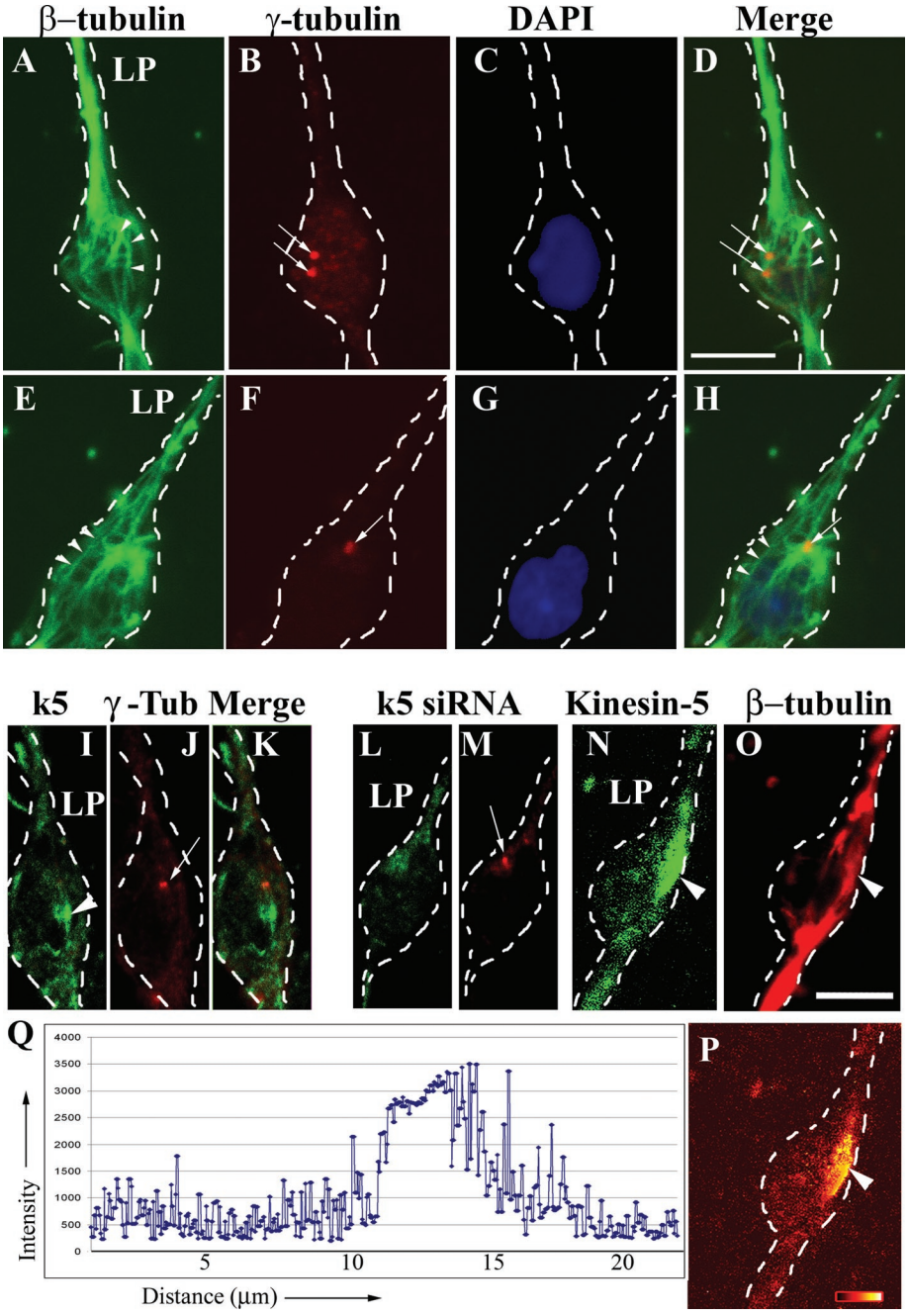

FIGURE 8: Immunostaining reveals centrosome-detached MTs and enrichment of kinesin-5 in the soma. (A–H) Two cultured cerebellar granule neurons triple-labeled for β-tubulin (green), γ–tubulin (red), and DAPI (blue) (Cell 1, top row; Cell 2, bottom row). The centrosome was situated on a side of the nucleus in Cell 1 (B and D, arrows) and ahead of the nucleus in Cell 2 (F and H, arrow). In both the cells, a subset of MTs extending into the leading process originated not at the centrosome but rather from a region behind the centrosome in the vicinity of the nucleus (A, D, E, and H, arrowheads). LP, leading process. Scale bar, 5 μm. (I, J, and K) A cultured cerebellar granule neuron double-stained for kinesin-5 (green) and γ-tubulin (red). (L and M) A cultured cerebellar granule neuron treated with kinesin-5 siRNA for 72 h, double-stained for kinesin-5 (green) and γ-tubulin (red). (N and O) A cultured cerebellar granule neuron double-stained for kinesin-5 (green) and β-tubulin (red). Scale bar, 5 μm. (P) Ratio image shown in glow-scale pseudocolor of this neuron. Black indicates the lowest ratio and white indicates the highest ratio of kinesin-5 to β-tubulin. Red, orange, and yellow indicate intermediate ratios. (Q) Quantitative intensity of a line profile through the ratio image shown in (P). Region behind the centrosome exhibits a higher ratio of kinesin-5 to MTs than many neighboring regions.

Enrichment of kinesin-5 in locales of potential anti-parallel MT organization

Our data on short MT transport complement previous observations indicating that not all MTs in migratory neurons are anchored to the centrosome. In these previous studies, conducted on neurons in cerebellar slices, a population of MTs was observed that extend into the leading process but with free ends originating from behind the centrosome, in the region of the nucleus (Umeshima *et al.*, 2007). To pursue this in our system, we immunostained cultured cerebellar migrating neurons for β-tubulin (to reveal MTs) and γ-tubulin (to reveal the centrosome), and analyzed the samples with confocal microscopy. Our results, similar to those of Umeshima and colleagues, indicate that although most of the MTs extending into the leading process originate from the centrosome, some do not (Figure 8, A, D, E, and H, arrowheads). This MT organization was observed whether the centrosome was situated ahead of the nucleus or on the side (N = 18).

If these MTs, free at both ends, were oriented oppositely to the rest in the leading process, then the leading process would clearly contain populations of anti-parallel MTs. Studies using GFP-EB3, however, have not revealed significant numbers of retrograde plus-end assembly excursions in leading processes (Tsai *et al.*, 2007), nor have MT polarity analyses revealed regions of nonuniformity of MT orientation in leading processes (Rakic *et al.*, 1996). Thus such MTs would have to have their plus ends directed into the leading processes and their minus ends directed behind the centrosome, creating regions of anti-parallel MT organization not in the leading process, but rather behind the centrosome where these free MTs would intermingle with MTs attached to the centrosome that extend back toward and around the nucleus.

Because kinesin-5 is a homotetramer known to function by generating forces between anti-parallel MTs, we next wanted to see whether the region behind the centrosome was particularly rich in kinesin-5. Therefore we immunostained cultures for kinesin-5, double-labeling either for β-tubulin (to reveal MTs) or γ-tubulin (to reveal the centrosome). For these studies we used an antibody specific for kinesin-5 in its phosphorylation state that favors binding to MTs (see Nadar *et al.*, 2008). Enrichments of kinesin-5 were observed in oval-shaped "hotspots" generally a few microns in length (Figure 8, I and N, arrowheads), and these hotspots were indeed consistently

situated behind the centrosome. These hotspots varied in size and were observed in ~86% of cells (n = 22), suggesting that kinesin-5 associates more strongly in certain locales of the neuron at various moments during migration to concentrate forces when and where needed. Confirming the specificity of the staining, these regions were absent from cells treated with kinesin-5 siRNA for 72 h (Figure 8L). Interestingly, in some cases, it was clear that the MT density within the kinesin-5 hotspots was no greater than that in the surrounding regions (Figure 8, O and P, arrowhead), indicating that the hotspots are not merely due to a greater density of MTs.

DISCUSSION

In the axon of a postmigratory neuron, all of the MTs are free at both ends and exist in a variety of lengths (Yu *et al.*, 1994). Short MTs are in rapid transit in both directions, whereas the longer stationary MTs are important for resisting compressive forces that would otherwise cause the axon to retract (Ahmad *et al.*, 2000; Myers *et al.*, 2006). Inhibition of kinesin-5 doubles the frequency of transport of the short MTs but also fortifies the resistance to axonal retraction provided by the long MTs (Myers and Baas, 2007). In the growth cone, kinesin-5 generates forces that oppose the entry of the longer MTs into filopodia, which is necessary for the appropriate turning of the growth cone in response to environmental cues (Nadar *et al.*, 2008). Collectively, the effects of kinesin-5 inhibition result in an axon that grows faster and retracts less, but does not turn properly. A useful analogy is to consider kinesin-5 as a "brake," both on the advance of the MT apparatus and on the growth of the axon itself. Without a proper brake, the growth of the axon is robust but uncontrolled.

The MT apparatus of a migrating neuron is distinctly different from that of a postmigratory neuron. The conventional view has been that most or all of the MTs throughout the migratory neuron remain attached to the centrosome and that centrosomal MTs traverse the entire length of the leading process. Recent studies using fluorescence imaging of +tips have shown that the plus ends of MTs in migratory neurons can be highly dynamic and that bouts of assembly and disassembly result in the intermittent and transient presence of plus ends of MTs throughout the leading process (Tsai *et al.*, 2007). With regard to minus-end attachment to the centrosome, our observations of short MTs moving anterogradely in the leading process demonstrate that at least some MTs are not attached to the centrosome. In migrating nonneuronal cells, long centrosomal MTs are important for tugging the centrosome along, but a population of short mobile MTs is also critically important. These short MTs are dispatched to the cell periphery to play an important functional role, presumably interacting with structures in the cell cortex (Abal *et al.*, 2002). With regard to migrating neurons, it is curious that the short mobile MTs are transported only anterogradely, as the transport is bidirectional in the axon. Perhaps this observation has something to do with the leading process being in motion as the short MTs move through it, as opposed to the axon being stationary. Nevertheless, similar to the case with the axon, the frequency of short MT transport in the leading process is enhanced by kinesin-5 inhibition. Notably, the leading process of the cerebellar granule neuron becomes the axon (Altman and Bayer, 1996), so it may be interesting to analyze the change in MT transport that occurs during this transition.

The most well-known manner by which kinesin-5 elicits its effects during mitosis is to generate forces between oppositely orientated MTs. Kinesin-5 is an extremely slow motor, as evidenced by the fact that it moves MTs in vitro more than 100 times slower than cytoplasmic dynein (Paschal *et al.*, 1987; Kapitein *et al.*, 2005). By moving so much more slowly, kinesin-5 inhibits the capacity of faster motors to do what they otherwise would. How this might work with regard to the axon has been a conundrum, because in the axon (and also the leading process of the migratory neuron; Rakic *et al.*, 1996) the MTs are uniformly oriented. One possibility is that the braking effect is localized more in the soma, where MTs have a variety of orientations (Liu *et al.*, 2010). In this view, short MTs may be present in the soma but immobilized through interactions with kinesin-5, and then made free to move on suppression of kinesin-5. With regard to longer MTs, confocal microscopy in our study and a previous study (Umeshima *et al.*, 2007) demonstrates that a subset of MTs in migratory neurons extend their plus ends into the leading process but have their minus ends situated behind the centrosome. These MTs would have the potential to intermingle with MTs of the opposite orientation emanating from the centrosome toward and around the nucleus. Such regions of oppositely oriented MTs would be ideal sites where the slower forces generated by kinesin-5 could act as a brake on the forces generated by cytoplasmic dynein (see Figure 9). Consistent with this mechanism, kinesin-5 is particularly enriched in locales that correspond to where such regions of anti-parallel MT organization would be expected to exist. Because neuronal migration involves forward movement of the MT cytoskeleton (Vallee *et al.*, 2009), it is possible that by "braking" the sliding of MTs along each other in these locales, kinesin-5 constrains the advance of the entire MT apparatus.

Inhibition of kinesin-5 results in a shorter leading process if the soma is migrating. If the soma is tightly adhered to the substrate, however, the situation becomes more akin to a neuron with an axon, with inhibition of kinesin-5 resulting in a longer leading process. Thus it may be that kinesin-5 compresses the leading process or axon toward the soma, and whether inhibition of kinesin-5 results in a longer or shorter leading process depends on whether the soma can move in response to the counterbalancing forces. As with the axon, the analogy of a brake is useful, with kinesin-5 acting to slow the rate of neuronal migration and to constrain the directionality of migration. When the levels of kinesin-5 are experimentally elevated, the neuron slows or even ceases migration altogether, probably because the brake reaches maximum strength. Consistent with this view, the highest levels of endogenous kinesin-5 are present when the neuron has reached its final destination.

The simplest mechanistic explanation for the various observations on the axon and on migrating neurons is that kinesin-5 generates forces that antagonize the effects of cytoplasmic dynein. Such a mechanism would be consistent with how kinesin-5 functions in the mitotic spindle, as well as cell extracts (Gaglio *et al.*, 1996; Rusan and Wadsworth, 2005). It also makes sense for how kinesin-5 impacts axonal growth and navigation, given that cytoplasmic dynein fuels the transport of short MTs (He *et al.*, 2005), enables the long MTs to resist actomyosin-based compressive forces (Ahmad *et al.*, 2000), and permits the MTs in the growth cone to enter filopodia by overcoming the retrograde flow of actin filaments (Myers *et al.*, 2006). Thus far, our observations in migratory neurons are also consistent with the impact of kinesin-5 inhibition being the opposite of the impact of inhibition of cytoplasmic dynein. Thus kinesin-5 may belong on a growing list of proteins that impinge on cytoplasmic dynein during neuronal migration (Mesngon *et al.*, 2006; Ayala *et al.*, 2007). Future efforts will be aimed at testing this idea and exploring potential functions in migratory neurons of other kinesins usually studied in the context of mitosis, such as kinesin-12 (Buster *et al.*, 2003; Liu *et al.*, 2010). We suspect that subtle differences in the mechanics of migration among different populations of neurons may relate to differences in how these MT-related motors are used and regulated.

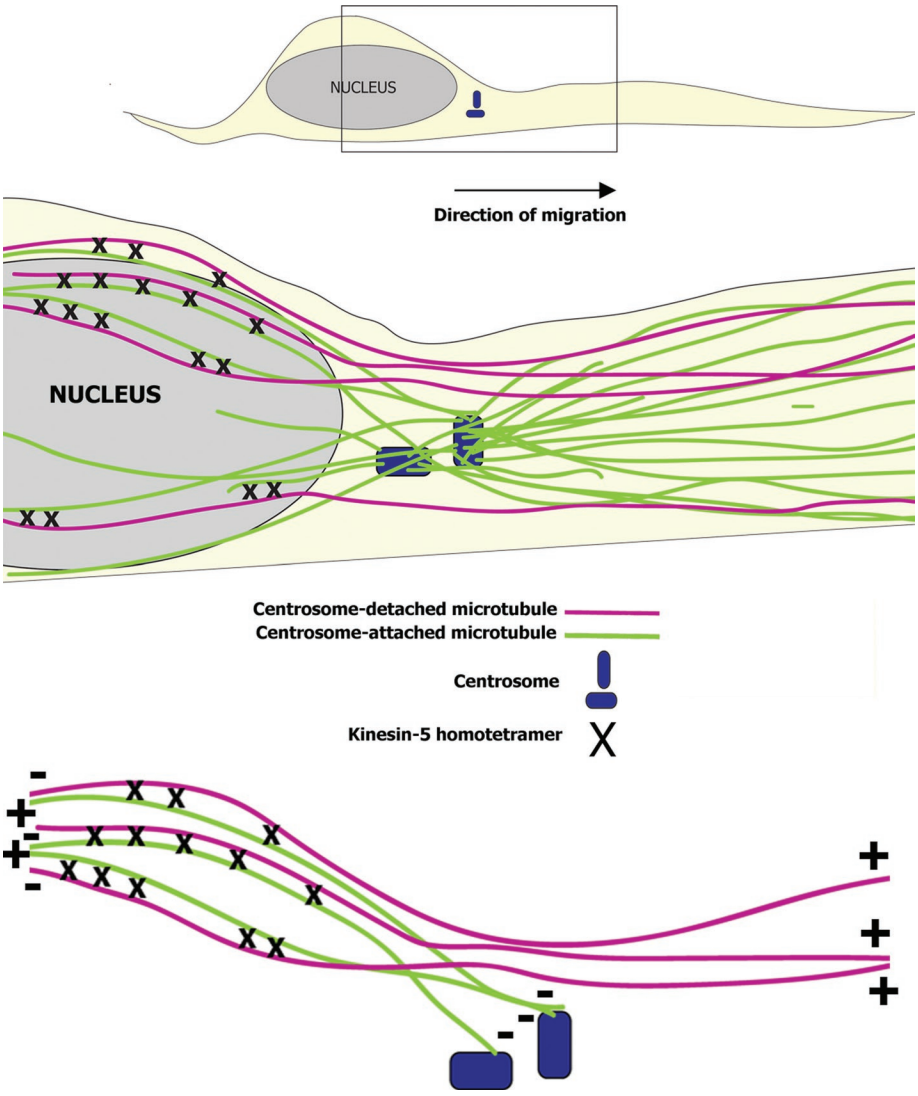

FIGURE 9: Schematized illustration depicting how kinesin-5–based forces may act during neuronal migration. Schematic illustration of a migrating neuron is shown at the top of the figure. A magnified subregion shown at the bottom of the figure includes the centrosome and part of the nucleus. MTs attached to the centrosome are shown as green lines. MTs that are not attached to the centrosome are shown as magenta lines. Green and magenta MTs intermingle behind the centrosome in anti-parallel (nonuniform MT polarity orientation) manner. Kinesin-5 homotetramers (shown as black crosses) generate forces in these regions of anti-parallel MT overlap that are much slower than the forces generated by cytoplasmic dynein. By virtue of its slower speed, kinesin-5 attenuates the rate at which cytoplasmic dynein can slide the MTs apart, and thereby regulates neuronal migration.

MATERIALS AND METHODS

Immunostaining of brain slices and cell cultures

p6-p8 rat pups were killed on ice by hypothermia. Cerebella were harvested and drop-fixed in 4% paraformaldehyde for 2 h. The tissue was equilibrated in 30% sucrose solution, embedded in M1 embedding matrix (Thermo Electron Corporation, Waltham, MA), frozen, and sliced into 15-µm-thick coronal sections on a Leica (St. Louis, MO) CM3000 cryostat. Sections were collected on glass slides coated with a solution of 6 g of gelatin and 0.4 g of chromium potassium sulfate in 308 ml of distilled water, 120 ml of 95% ethanol, and 28 ml of glacial acetic acid; allowed to dry for 2 h; washed repeatedly with 1× phosphate-buffered saline (PBS) (Fisher BioReagents, Fair Lawn, NJ); blocked with 10% normal goat serum (Jackson ImmunoResearch Labs, West Grove, PA) and 0.02% Triton X-100 (Sigma, St. Louis, MO) in 1× PBS for 1 h; incubated at 4°C overnight with primary antibody made in 5% normal goat serum and 0.02% Triton X-100; rinsed the next day with 1× PBS; then incubated for 1 h at room temperature with fluorescent secondary antibody made in 5% goat serum in 1× PBS. VECTASHIELD (Vector Laboratories, Burlingame, CA) was used to protect fluorescence from fading. For cultures of migrating neurons, the neurons were rapidly fixed with methanol that had been chilled for 24 h at –20°C. Blocking and other staining procedures were identical to those for brain slices. Sections of developing cerebral cortex were also prepared and stained as just described. For these experiments, brains were harvested from embryonic rats on the 16th day of gestation (E16) as described elsewhere (Qiang *et al.*, 2010).

A polyclonal antibody for kinesin-5 (Cocalico Biologicals, Reamstown, PA) that had been raised in rabbit using a synthetic peptide sequence from the tail domain of rat kinesin-5 (amino acid residues 801–991, GenBank accession number NP_001162583) was used at a 1:500 dilution as a primary antibody for immunostaining sections. For visualizing sites of kinesin-5 interaction with MTs in cultured neurons, we used a phosphospecific kinesin-5 antibody raised in rabbit (PhosphoSolutions, Aurora, CO) at a 1:500 dilution. We used another antibody specific for total kinesin-5 to confirm results obtained using the above-mentioned total-kinesin-5–specific antibody (Nadar *et al.*, 2008). For eGFP staining, a rabbit polyclonal GFP antibody (Sigma, St. Louis, MO) was used at a 1:400 dilution. For MT staining, a mouse monoclonal β-tubulin antibody (Sigma) at a 1:400 dilution or a mouse monoclonal α-tubulin antibody (Sigma) at a 1:400 dilution was used. For centrosome staining, a rabbit polyclonal-γ-tubulin antibody (Sigma) at a 1:800 dilution was used. A Cy3-conjugated goat anti-mouse antibody (Jackson ImmunoResearch, West Grove, PA) and Alexa Fluor 488–conjugated goat anti-rabbit antibody (Invitrogen, Carlsbad, CA) were used at a 1:400 dilution as secondary antibodies.

Images of immunostained tissue sections were acquired using the Axiovert 200M microscope controlled by AxioVision 4.6 software (Carl Zeiss, Thornwood, NY). Images were captured using 10× and 40× objectives. Image acquisition for cultured granule neurons was performed using a Zeiss confocal microscope, controlled by LSM5 Pascal software. The pinhole was set to obtain optical sections with a thickness of 2 µm.

In vitro neuronal migration assay

We used an in vitro culture system of rat cerebellar granule neurons, which has been used in the past to study the cytoskeletal mechanisms underlying neuronal migration (Bix and Clark, 1998; Hirotsune

et al., 1998; He *et al.*, 2010; Peng *et al.*, 2010; Tahirovic *et al.*, 2010). Cerebella were harvested from p6-p8 rats, dissociated by trituration to form a single cell suspension, and then allowed to stand overnight in a polypropylene tube during which time cells reaggregated. The next day, the cerebellar reaggregates were plated on laminin-coated glass coverslips. More than 90% of cells in these cultures stain positive with anti-neurofilament antibody and are spindle-shaped bipolar cells measuring ~6 µm in diameter, indicating that they are indeed cerebellar granule neurons (Altman, 1972; Selak *et al.*, 1985; Gilad *et al.*, 1989). Cellular reaggregates were plated in serum-containing medium on laminin-coated coverslips. The presence of serum suppressed neurite outgrowth (Liesi, 1992). One hour after plating, aggregates adhered to the substrate, at which point, the plating medium was replaced by serum-free medium. Within an hour after this, cellular processes extending out of the periphery of the aggregate were visible, and bipolar cells, which extended their leading processes along these preextended "pioneer" neurites, began translocating out of the aggregates (Asou *et al.*, 1992). The laminin substrate on which the cells were plated is known to be sufficient by itself as an adhesion molecule on which granule neurons are able to migrate in vitro without requiring any other guidance cue (Liesi, 1992; Bix and Clark, 1998). Also, in vivo, the cell adhesion molecule L1, expressed by granule neurons, and the extracellular matrix molecule laminin, produced by Bergman glia, are known to be involved in migration of granule neurons (Lindner *et al.*, 1983; Liesi, 1985, 1992). Thus there is reasonable confidence that neurons undergo a single mode of in vitro migration, which is independent of glial cells.

Within the first 4–6 h, while outward bound migrating granule neurons are still in contact with the periphery of the aggregate, the aggregate appears to grow in size. Later, as more neurons migrate out of the aggregate and move farther away, the aggregate shrinks in size. For aggregate size comparison experiments, aggregates were photographed at 4 h and at 6–7 h after plating, using 10× phase-contrast optics. For live-cell imaging on individual migrating granule neurons, 24 h after plating, coverslips were placed in a live-cell imaging workstation consisting of a Zeiss inverted "Observer" microscope with an Orca II ER CCD (Hamamatsu, Japan) and a Zeiss incubation chamber. Serial images were captured at 3-min intervals using a 40× phase-contrast objective.

For kinesin-5 inhibition experiments, 2 µl of 100 µM monastrol (Sigma) solution in DMSO (Sigma) or 2 µl of DMSO alone were added to 2 ml of serum-free medium, and this solution was applied to cells at least 1 h before recording. For siRNA studies, freshly isolated p5 granule neurons were transfected with 10 µM control or kinesin-5 siRNA (Silencer KIF11 [Eg5] siRNA; Ambion, Foster City, CA) using the Amaxa Nucleofector II, plated densely on PLL-coated plastic dishes (1 mg/ml PLL, 1 ml/dish for 12 h at 4°C and repeatedly rinsed in double-distilled H_2O) for 60 h, then trypsinized and allowed to incubate overnight so as to form aggregates. The aggregates were plated the next day (72-h point), and observations were made as described earlier in this section. Seventy-two hours is sufficient time for this siRNA to deplete >85% of the kinesin-5 protein as determined by Western blotting and as shown previously (Myers and Baas, 2007).

Morphological analyses of the leading process length

Dissociated cerebellar cells were obtained from p6-p8 rat pups as mentioned earlier in the text, transfected with eGFP-N1 (Clontech, Mountain View, CA), and densely plated on PLL-coated plastic dishes for ~12 h. Then they were trypsinized, aggregated, and replated on laminin-coated glass coverslips, were allowed to migrate, and were plated either on laminin-coated glass coverslips (25 µg/ml laminin, 200 ml per coverslip for 12 h) for 24 h or on PLL-coated coverslips (1 mg/ml PLL, 1 ml/dish for 12 h at 4°C and repeatedly rinsed in double-distilled H_2O) and treated with 2.5 µg/ml laminin (total 2 ml) for 20 h. Next, either 100 µM solution of monastrol in DMSO or DMSO alone was added to the medium for 4 h. Neuronal migration was recorded using time-lapse imaging for at least 30 min. Leading process lengths of migrating neurons were measured using the "measure/curve" application of AxioVision LE 4.5 (Carl Zeiss MicroImaging), and mean values were quantified. For kinesin-5 overexpression experiments, we used eGFP–kinesin-5 as described previously (Myers and Baas, 2007). For these experiments, ~1 million dissociated cerebellar cells were transfected with 15 µg of either kinesin-5–eGFP or EGFP alone, densely plated on PLL-coated plastic dishes for 24 h, trypsinized and replated more sparsely on laminin-coated glass coverslips for 24 h, and processed further as described earlier in the text.

Live-cell imaging of MT transport

The photo-bleaching–based MT transport assay was performed as described previously (He *et al.*, 2005; Myers and Baas, 2007). P5 cerebellar granule neurons were isolated as mentioned earlier in the text. Approximately 1 million cells were transfected with 15 µg of eGFP–tubulin (Clontech Laboratories) using the Amaxa Nucleofector II, densely plated on PLL-coated plastic dishes for ~12 h, trypsinized and replated on laminin-coated glass coverslips, and allowed to migrate. A coverslip was then placed in a live-cell imaging workstation consisting of an inverted "Observer" microscope, an Orca II ER CCD (Hamamatsu, Japan), and a FluoArc Mercury lamp system, all controlled by AxioVision 4.1 software (Zeiss), with a Zeiss incubation chamber, interfaced with the MicroPoint Mosaic Digital Diaphragm system from Photonics Instruments (South Windsor, CT), coupled to an argon ion laser. The Zeiss incubation chamber provides optimal conditions of 37°C and 5% CO_2. The Mosaic system is able, with great precision, to deliver a sharp laser pulse on to a predetermined target region of a cell. Prior to photo-bleaching, an eGFP—tubulin–expressing neuron was identified, and its migration was recorded using a 40× objective with phase-contrast optics and by capturing serial images at 3-min intervals, for a total period of 30 min. After ascertaining the migrating state of a neuron, a 15-µm stretch of its leading process was exposed to the laser for 3 ms to bleach the eGFP fluorescence in that region. For the next 3 min, rapid serial images were captured at 2-s intervals, using 200-ms exposure and a 100× objective with fluorescence optics to track the movement of short fluorescent MTs against the dark background of the bleached zone. For kinesin-5 inhibition experiments, either 100 µM solution of monastrol in DMSO or DMSO alone was added to the medium, at least 45 min before recording migration. For quantification, we manually tracked all of the fluorescent MTs that exhibited movement resulting in net displacement through the bleached zone. Transport frequency was calculated by dividing the total number of movements by the total imaging time. Transport velocity was calculated by dividing the total distance traveled by the MT by time taken for the movement.

In utero electroporation

The procedure for in utero electroporation was performed as described elsewhere (Saito and Nakatsuji, 2001). Briefly, 2.5% avertin (2,2,2-tribromoethanol, 97% in *tert*-amylalcohol [Sigma-Aldrich, St. Louis, MO]) dissolved in 0.9% saline was injected intraperitoneally (15 µl/g of body weight of the mouse) to anesthetize

timed-pregnant mice at E14. Approximately 3–5 μl of DNA solution prepared using QIAGEN (Chatsworth, CA) Plasmid Maxi Kit, was injected into the lateral ventricle using a fine glass capillary. Electroporation was performed using BTX ECM 830 Electro Square Porator (30 V, 5 pulses, 50-ms pulse length, 1.0-s interval; BTX Instrument, Holliston, MA). Uterine horns were repositioned into the abdominal cavity, and the abdominal wall and skin were sewed up with surgical sutures. Mice were kept on a warm plate (37°C) for recovery. Mice were killed, brains were harvested at P1, and the brains of electroporated embryos were sectioned then stained with the GFP antibody. Fluorescence images were acquired with the Zeiss Axiovert 200M. For in utero electroporation, the eGFP–kinesin-5 construct was made by inserting the kinesin-5–EGFP sequence between *Eco*RI and *Not*I sites in the pEF vector (Elongation Factor-1 α promoter). The pEF-GFP construct was used as control.

ACKNOWLEDGMENTS

For helpful discussions, we thank B. Timothy Himes, Wenqian Yu, Mei Liu, Vidya Nadar, and Joanna Solowska of Drexel University and Douglas Baird of Temple University. We are grateful to Kranti Kadam and the Tata Institute Animal Facility for assistance with the in utero electroporation experiments. We especially thank Orly Reiner of Weizmann Institute for critically reading the manuscript and Judy Liu of Children's National Medical Center for critical comments on the figures. This work was supported by grants from the National Institutes of Health, the National Science Foundation, and Pennsylvania Tobacco Settlement Funds (to P.W.B.). Aditi Falnikar is the recipient of the Doris Willig, M.D., Award from Drexel University College of Medicine, Institute for Women's Health and Leadership. Shubha Tole is the recipient of the Shanti Swarup Bhatnagar prize.

REFERENCES

Abal M, Piel M, Bouckson-Castaing V, Mogensen M, Sibarita JB, Bornens M (2002). Microtubule release from the centrosome in migrating cells. J Cell Biol 159, 731–737.

Ahmad FJ, Hughey J, Wittmann T, Hyman A, Greaser M, Baas PW (2000). Motor proteins regulate force interactions between microtubules and microfilaments in the axon. Nat Cell Biol 2, 276–280.

Altman J (1969). Autoradiographic and histological studies of postnatal neurogenesis. 3. Dating the time of production and onset of differentiation of cerebellar microneurons in rats. J Comp Neurol 136, 269–293.

Altman J (1972). Postnatal development of the cerebellar cortex in the rat. I. The external germinal layer and the transitional molecular layer. J Comp Neurol 145, 353–397.

Altman J, Bayer SA (1996). Development of the Cerebellar System in Relation to Its Evolution, Structure, and Functions, Boca Raton, FL: CRC Press.

Asou H, Miura M, Kobayashi M, Uyemura K, Itoh K (1992). Cell adhesion molecule L1 guides cell migration in primary reaggregation cultures of mouse cerebellar cells. Neurosci Lett 144, 221–224.

Ayala R, Shu T, Tsai LH (2007). Trekking across the brain: the journey of neuronal migration. Cell 128, 29–43.

Bellion A, Baudoin JP, Alvarez C, Bornens M, Metin C (2005). Nucleokinesis in tangentially migrating neurons comprises two alternating phases: forward migration of the Golgi/centrosome associated with centrosome splitting and myosin contraction at the rear. J Neurosci 25, 5691–5699.

Bix GJ, Clark GD (1998). Platelet-activating factor receptor stimulation disrupts neuronal migration in vitro. J Neurosci 18, 307–318.

Buster DW, Baird DH, Yu W, Solowska JM, Chauviere M, Mazurek A, Kress M, Baas PW (2003). Expression of the mitotic kinesin Kif15 in postmitotic neurons: implications for neuronal migration and development. J Neurocytol 32, 79–96.

Cochran JC, Gilbert SP (2005). ATPase mechanism of Eg5 in the absence of microtubules: insight into microtubule activation and allosteric inhibition by monastrol. Biochemistry 44, 16633–16648.

Distel M, Hocking JC, Volkmann K, Koster RW (2010). The centrosome neither persistently leads migration nor determines the site of axonogenesis in migrating neurons in vivo. J Cell Biol 191, 875–890.

Ferhat L, Cook C, Chauviere M, Harper M, Kress M, Lyons GE, Baas PW (1998). Expression of the mitotic motor protein Eg5 in postmitotic neurons: implications for neuronal development. J Neurosci 18, 7822–7835.

Gaglio T, Saredi A, Bingham JB, Hasbani MJ, Gill SR, Schroer TA, Compton DA (1996). Opposing motor activities are required for the organization of the mammalian mitotic spindle pole. J Cell Biol 135, 399–414.

Gilad GM, Gilad VH, Dahl D (1989). Expression of neurofilament immunoreactivity in developing rat cerebellum in vitro and in vivo. Neurosci Lett 96, 7–12.

Gregory WA, Edmondson JC, Hatten ME, Mason CA (1988). Cytology and neuron-glial apposition of migrating cerebellar granule cells in vitro. J Neurosci 8, 1728–1738.

Haque SA, Hasaka TP, Brooks AD, Lobanov PV, Baas PW (2004). Monastrol, a prototype anti-cancer drug that inhibits a mitotic kinesin, induces rapid bursts of axonal outgrowth from cultured postmitotic neurons. Cell Motil Cytoskeleton 58, 10–16.

Hasaka TP, Myers KA, Baas PW (2004). Role of actin filaments in the axonal transport of microtubules. J Neurosci 24, 11291–11301.

Hatten ME, Mason CA (1990). Mechanisms of glial-guided neuronal migration in vitro and in vivo. Experientia 46, 907–916.

He M, Zhang ZH, Guan CB, Xia D, Yuan XB (2010). Leading tip drives soma translocation via forward F-actin flow during neuronal migration. J Neurosci 30, 10885–10898.

He Y, Frances F, Myers KA, Black M, Baas PW (2005). Role of cytoplasmic dynein in the axonal transport of microtubules and neurofilaments. J Cell Biol 168, 697–703.

Hirotsune S, Fleck MW, Gambello MJ, Bix GJ, Chen A, Clark GD, Ledbetter DH, McBain CJ, Wynshaw-Boris A (1998). Graded reduction of Pafah1b1 (Lis1) activity results in neuronal migration defects and early embryonic lethality. Nat Genet 19, 333–339.

Jaglin XH, Chelly J (2009). Tubulin-related cortical dysgenesis: microtubule dysfunction underlying neuronal migration defects. Trends Genet 25, 555–566.

Jaglin XH *et al.* (2009). Mutations in the beta-tubulin gene TUBB2B result in asymmetrical polymicrogyria. Nat Genet 41, 746–752.

Kapitein LC, Peterman EJ, Kwok BH, Kim JH, Kapoor TM, Schmidt CF (2005). The bipolar mitotic kinesin Eg5 moves on both microtubules that it cross-links. Nature 435, 114–118.

Keays DA *et al.* (2007). Mutations in alpha-tubulin cause abnormal neuronal migration in mice and lissencephaly in humans. Cell 128, 45–57.

Liesi P (1985). Do neurons in the vertebrate CNS migrate on laminin? EMBO J 4, 1163–1170.

Liesi P (1992). Neuronal migration on laminin involves neuronal contact formation followed by nuclear movement inside a preformed process. Exp Neurol 117, 103–113.

Lindner J, Rathjen FG, Schachner M (1983). L1 mono- and polyclonal antibodies modify cell migration in early postnatal mouse cerebellum. Nature 305, 427–430.

Liu M, Nadar VC, Kozielski F, Kozlowska M, Yu W, Baas PW (2010). Kinesin-12, a mitotic microtubule-associated motor protein, impacts axonal growth, navigation, and branching. J Neurosci 30, 14896–14906.

Martini FJ, Valdeolmillos M (2010). Actomyosin contraction at the cell rear drives nuclear translocation in migrating cortical interneurons. J Neurosci 30, 8660–8670.

Mesngon MT, Tarricone C, Hebbar S, Guillotte AM, Schmitt EW, Lanier L, Musacchio A, King SJ, Smith DS (2006). Regulation of cytoplasmic dynein ATPase by Lis1. J Neurosci 26, 2132–2139.

Myers KA, Baas PW (2007). Kinesin-5 regulates the growth of the axon by acting as a brake on its microtubule array. J Cell Biol 178, 1081–1091.

Myers KA, Tint I, Nadar CV, He Y, Black MM, Baas PW (2006). Antagonistic forces generated by cytoplasmic dynein and myosin-II during growth cone turning and axonal retraction. Traffic 7, 1333–1351.

Nadar VC, Ketschek A, Myers KA, Gallo G, Baas PW (2008). Kinesin-5 is essential for growth cone turning. Curr Biol 18, 1972–1977.

Paschal BM, King SM, Moss AG, Collins CA, Vallee RB, Witman GB (1987). Isolated flagellar outer arm dynein translocates brain microtubules in vitro. Nature 330, 672–674.

Peng YJ *et al*. (2010). Trio is a key guanine nucleotide exchange factor coordinating regulation of the migration and morphogenesis of granule cells in the developing cerebellum. J Biol Chem 285, 24834–24844.
Qiang L, Yu W, Liu M, Solowska JM, Baas PW (2010). Basic fibroblast growth factor elicits formation of interstitial axonal branches via enhanced severing of microtubules. Mol Biol Cell 21, 334–344.
Rakic P, Knyihar-Csillik E, Csillik B (1996). Polarity of microtubule assemblies during neuronal cell migration. Proc Natl Acad Sci USA 93, 9218–9222.
Rusan NM, Wadsworth P (2005). Centrosome fragments and microtubules are transported asymmetrically away from division plane in anaphase. J Cell Biol 168, 21–28.
Saito T, Nakatsuji N (2001). Efficient gene transfer into the embryonic mouse brain using in vivo electroporation. Dev Biol 240, 237–246.
Saunders AM, Powers J, Strome S, Saxton WM (2007). Kinesin-5 acts as a brake in anaphase spindle elongation. Curr Biol 17, R453–R454.
Schaar BT, McConnell SK (2005). Cytoskeletal coordination during neuronal migration. Proc Natl Acad Sci USA 102, 13652–13657.
Selak I, Foidart JM, Moonen G (1985). Laminin promotes cerebellar granule cells migration in vitro and is synthesized by cultured astrocytes. Dev Neurosci 7, 278–285.
Sharp DJ, Rogers GC, Scholey JM (2000). Microtubule motors in mitosis. Nature 407, 41–47.
Sheppard AM, Pearlman AL (1997). Abnormal reorganization of preplate neurons and their associated extracellular matrix: an early manifestation of altered neocortical development in the reeler mutant mouse. J Comp Neurol 378, 173–179.
Sidman RL, Rakic P (1973). Neuronal migration, with special reference to developing human brain: a review. Brain Res 62, 1–35.
Solecki DJ, Model L, Gaetz J, Kapoor TM, Hatten ME (2004). Par6alpha signaling controls glial-guided neuronal migration. Nat Neurosci 7, 1195–1203.
Solecki DJ, Trivedi N, Govek EE, Kerekes RA, Gleason SS, Hatten ME (2009). Myosin II motors and F-actin dynamics drive the coordinated movement of the centrosome and soma during CNS glial-guided neuronal migration. Neuron 63, 63–80.
Tahirovic S, Hellal F, Neukirchen D, Hindges R, Garvalov BK, Flynn KC, Stradal TE, Chrostek-Grashoff A, Brakebusch C, Bradke F (2010). Rac1 regulates neuronal polarization through the WAVE complex. J Neurosci 30, 6930–6943.
Tanaka T, Serneo FF, Higgins C, Gambello MJ, Wynshaw-Boris A, Gleeson JG (2004). Lis1 and doublecortin function with dynein to mediate coupling of the nucleus to the centrosome in neuronal migration. J Cell Biol 165, 709–721.
Tsai JW, Bremner KH, Vallee RB (2007). Dual subcellular roles for LIS1 and dynein in radial neuronal migration in live brain tissue. Nat Neurosci 10, 970–979.
Tsai JW, Chen Y, Kriegstein AR, Vallee RB (2005). LIS1 RNA interference blocks neural stem cell division, morphogenesis, and motility at multiple stages. J Cell Biol 170, 935–945.
Tsai LH, Gleeson JG (2005). Nucleokinesis in neuronal migration. Neuron 46, 383–388.
Umeshima H, Hirano T, Kengaku M (2007). Microtubule-based nuclear movement occurs independently of centrosome positioning in migrating neurons. Proc Natl Acad Sci USA 104, 16182–16187.
Vallee RB, Seale GE, Tsai JW (2009). Emerging roles for myosin II and cytoplasmic dynein in migrating neurons and growth cones. Trends Cell Biol 19, 347–355.
Wang L, Brown A (2002). Rapid movement of microtubules in axons. Curr Biol 12, 1496–1501.
Yoon SY, Choi JE, Huh JW, Hwang O, Lee HS, Hong HN, Kim D (2005). Monastrol, a selective inhibitor of the mitotic kinesin Eg5, induces a distinctive growth profile of dendrites and axons in primary cortical neuron cultures. Cell Motil Cytoskeleton 60, 181–190.
Yu W, Ahmad FJ, Baas PW (1994). Microtubule fragmentation and partitioning in the axon during collateral branch formation. J Neurosci 14, 5872–5884.